Silicon nanowire based high brightness, pulsed relativistic electron source

Deep Sarkar,[1,a] Prashant Kumar Singh,[1] G. Cristoforetti,[2,a] Amitava Adak,[1] Gourab Chatterjee,[1] Moniruzzaman Shaikh,[1] Amit D. Lad,[1] P. Londrillo,[2] Giuseppe D'Arrigo,[3] J. Jha,[1] M. Krishnamurthy,[4] L. A. Gizzi,[2] and G. Ravindra Kumar[1,a]

[1]*Tata Institute of Fundamental Research, Mumbai, India*
[2]*ILIL, National Institute of Optics, CNR, Pisa, Italy*
[3]*CNR-Institute for Microelectronics and Microsystems, Catania, Italy*
[4]*Tata Institute of Fundamental Research, Hyderabad, India*

(Received 28 March 2017; accepted 22 May 2017; published online 9 June 2017)

We demonstrate that silicon nanowire arrays efficiently emit relativistic electron pulses under irradiation by a high-intensity, femtosecond, and near-infrared laser ($\sim 10^{18}$ W/cm^2, 25 fs, 800 nm). The nanowire array yields fluxes and charge per bunch that are 40 times higher than those emitted by an optically flat surface, in the energy range of 0.2–0.5 MeV. The flux and charge yields for the nanowires are observed to be directional in nature unlike that for planar silicon. Particle-in-cell simulations establish that such large emission is caused by the enhancement of the local electric fields around a nanowire, which consequently leads to an enhanced absorption of laser energy. We show that the high-intensity contrast (ratio of picosecond pedestal to femtosecond peak) of the laser pulse (10^{-9}) is crucial to this large yield. We extend the notion of surface local-field enhancement, normally invoked in low-order nonlinear optical processes like second harmonic generation, optical limiting, etc., to ultrahigh laser intensities. These electron pulses, expectedly femtosecond in duration, have potential application in imaging, material modification, ultrafast dynamics, terahertz generation, and fast ion sources. [http://dx.doi.org/10.1063/1.4984906]

I. INTRODUCTION

Ultrashort, relativistic electron bunches are created when an intense laser pulse interacts with a solid. Such electrons are emitted both at the target front and rear and carry information on laser absorption by the target and electron transport in the hot, dense matter, created by the propagation[1–5] of these electron bunches. Nanostructures are versatile in their ability for efficient light coupling to solids at low incident intensities, thereby enhancing various processes, namely, second harmonic generation,[6] surface-enhanced Raman spectroscopy (SERS),[7,8] optical limiting,[9] multi-photon emission, etc. It is of considerable practical interest to explore if nanostructures facilitate such enhancement at ultra-high laser intensities in view of the potential application of the high-energy electron bunches[10] in the studies on ultrafast electron microscopy and as sources of high-energy X-rays,[11] THz radiation,[12] and fast ion beams.[13,14] These radiation sources are indispensable tools for ultrafast imaging,[15] spectroscopy,[16] cancer therapy,[17,18] and material science.[19] Studies have shown that increased X-ray emission is achieved when moderately high-intensity (10^{16} W/cm^2), femtosecond laser pulses interact with nanostructures.[20] It is still an open question whether such enhancements occur at higher intensities[21] since the structures may be damaged by the rising edges of the high-intensity pulse and may not survive long enough to interact with the peak intensity.

[a]Electronic addresses: deep.sarkar@tifr.res.in; gabriele.cristoforetti@cnr.it; and grk@tifr.res.in

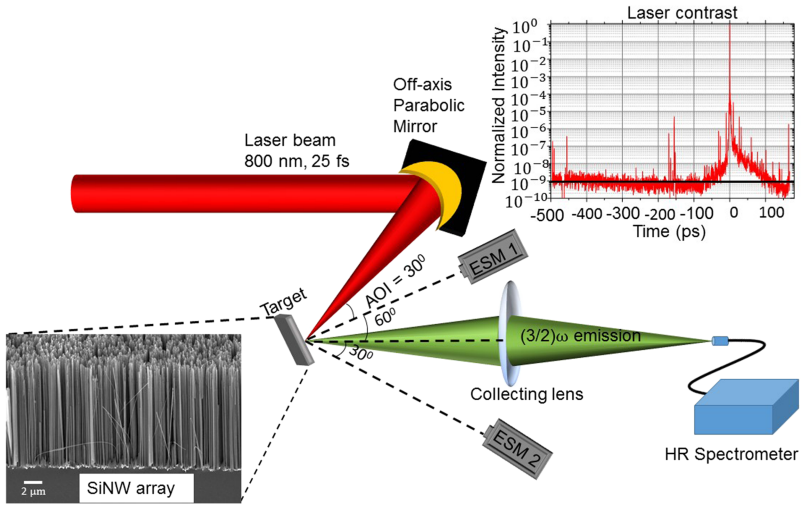

FIG. 1. Schematic for the experimental setup. The laser beam is focused on the target with an (f/2.5) off-axis parabola (OAP). Electron Spectrometers (ESM) are used for the measurement of the electron energy spectrum. The (3/2)ω emission from plasma is captured using a high-resolution, compact UV-visible spectrometer. (Inset) SEM image of the SiNW array and laser intensity profile.

In order for the laser pulse to "see" the nanostructures on the target, the structural dimensions must be of the same order as the characteristic length scales affecting the interaction—for instance, the collisionless skin depth, the quiver amplitude of the electrons oscillating in the laser field, the laser wavelength, and the pre-plasma density scale length. If the nanostructure dimensions are well below these length scales, the laser pulse would effectively "see" a plane target and the enhanced coupling due to structuring can no longer be expected. It is, however, difficult to experimentally investigate the nature of the interaction by tuning the target parameters owing to the difficulty inherent in the fabrication of structured targets with tunable dimensions. Another important factor determining the nature of the laser-matter interaction and the efficiency of laser absorption is the temporal structure of the laser pulse. The possibility of an early onset of ionization and the formation of a plasma prior to the arrival of the main peak is the result of such a low-intensity pedestal of several picoseconds accompanying the main peak. This can damage the structures well before the main peak of the pulse arrives. Another challenging aspect of the problem is the fact that the ablation threshold for nanostructured targets is much lower than the plane targets due to their higher absorption efficiency.[22]

In this letter, we show that silicon nanowire (SiNW) arrays[23] enhance the interaction with high contrast, high-intensity laser pulses, and generate high-flux relativistic electron pulses in the energy range of 0.2–0.5 MeV. The flux is also found to be dependent on the emission direction—a feature not observed in the planar case. We demonstrate local light field enhancement, normally observed at low intensities of light, in the regime of ultrahigh intensities[24] (10^{18} W/cm^2). Silicon nanowires were fabricated using a bottom-up approach with random silver deposition and silicon etching in two separate steps. In the first step, the samples were immersed in a solution of 0.005M $AgNO_3$ and 4.8M HF for 160 s to promote the silver nanocluster deposition on the Si (100) surface, and in the next step, they were immersed in a second solution of 0.1M H_2O_2 and 4.8M HF for 30 min to activate the silicon etching. A Scanning Electron Microscope (SEM) image of the nanowire arrays used for the experiment is shown in the inset of Fig. 1. The nanowires were ~8 μm in length and ~10–20 nm in diameter, randomly distributed on the surface with inter-wire separation ~10–50 nm, giving a fill factor in the range of 0.04–0.2.

II. EXPERIMENT

The experiments were carried out using the 100 TW Ti:Sapphire chirped pulse amplification[25] laser system at the Tata Institute of Fundamental Research (TIFR), Mumbai. As shown in Fig. 1,

the laser beam (800 nm, 25 fs) was focused on the target in p-polarization at an incidence angle of 30° to a spot size of 10 μm × 15 μm (full width at half maximum) by an (f/2.5) off-axis parabolic mirror. The intensity on the target was varied in the range $I\lambda^2 = (1.5–3) \times 10^{18}$ W μm^2 cm^{-2}.

The ratio of the main peak intensity to the pedestal intensity, known as pulse contrast, is measured by third order cross-correlation techniques and is shown in the inset of Fig. 1. The contrast ratio of the main peak with respect to the nanosecond-long pedestal (due to amplified spontaneous emission) was $\sim 10^{-9}$, while it was $\sim 10^{-6}$ at 3 ps before the main peak.

The plasma created at the target surface was probed by electron and optical spectrometers. A high-resolution, fiber-coupled spectrometer [$\Delta\lambda = (350–800)$ nm] measured the emission spectrum along the specular direction, sent to it through a fiber. This was aimed at detecting the three-halves harmonic emission ($\lambda \sim 532$ nm) and second harmonic emission ($\lambda \sim 400$ nm), the former resulting from the Two Plasmon Decay (TPD)[22] instability in the under-dense ($n < n_c$) plasma region at a layer of density $\frac{n_c}{4}$. Since TPD requires an appreciable pre-plasma scale length ($\sim \lambda_{laser}$) to grow,[26,27] the detection of the $(3/2)\omega_0$ signal could be used to indicate the presence of a pre-plasma. However, no such (3/2) harmonic emission was observed for the nanowire arrays at any laser irradiance, indicating that these structures survived during the irradiation of pre-pulse.

To measure the spectra of the relativistic electrons, two magnet-based electron spectrometers (ESM)[28] were placed at angles of 0° and 60° with respect to the target normal (shown in Fig. 1) at distances of 22 cm ($\theta = 0°$) and 21.5 cm ($\theta = 60°$), respectively. The laser-generated electrons are made to pass through a narrow collimating aperture of diameter ~2 mm before it reaches the detector plate.

III. RESULTS AND DISCUSSION

In our experiments, we characterize the electrons emitted at the front of the target and compare their spectra with those obtained for a plane silicon target. The electrons at the front are chosen for

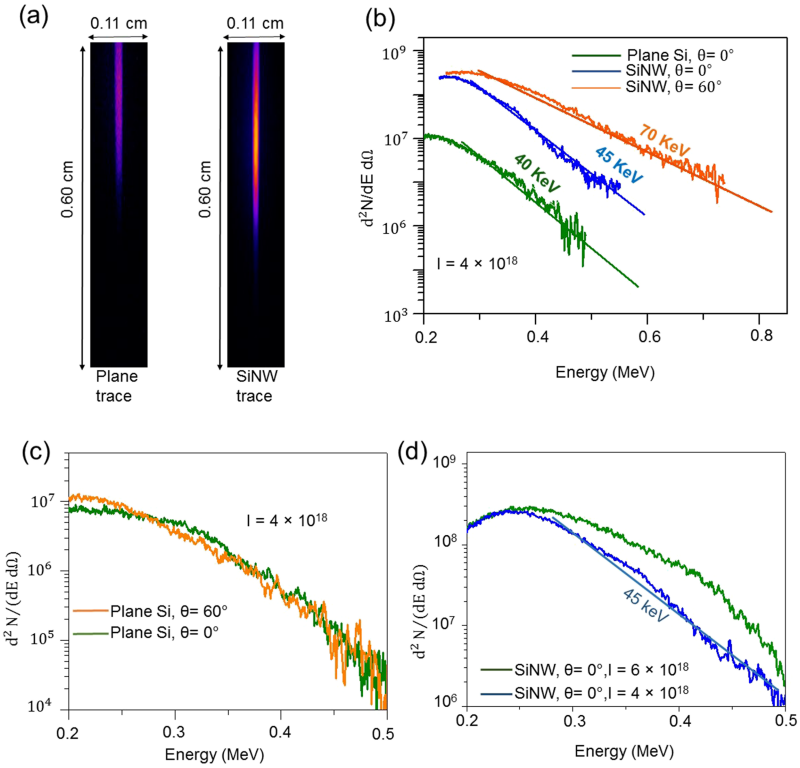

FIG. 2. (a) Front side ESM traces for plane Si and SiNW. (b) Electron energy spectra for plane ($\theta = 0°$) and SiNW target ($\theta = 60°$). (c) Electron energy spectra for plane Si for $\theta = 0°$ and $\theta = 60°$. (d) Energy spectra for SiNW at $\theta = 0°$ for two different intensities. All intensity values are in units of W/cm^2.

the analysis as they do not interact with the bulk of the target and hence can be compared more easily with the simulation results.

Energy spectra of the relativistic electrons emitted from nanowire targets revealed a much higher total yield compared to the plane silicon case, as shown in Fig. 2. The electron temperature for the nanowire arrays (70 keV) is also observed to be higher than that of a plane silicon target (40 keV), although along the target normal direction (45 keV), the enhancement is within the limits of the measurement uncertainty. The flux enhancement along 0° is 20 times while that along $\theta = 60°$ is 40 times, indicating an anisotropic distribution of the relativistic electrons. Since the charge yield per bunch is linearly related to the flux ($Q = e \times$ flux), the charge enhancement factor remains the same (along 0°, 2.4 pC for flat and 58 pC for nanowires; along $\theta = 60°$, 2.6 pC for flat and 114 pC for nanowires). These data indicate a clear anisotropy in the case of the nanowire arrays.

IV. COMPUTATIONAL ANALYSIS

To comprehend these experimental results and have a closer look at the underlying mechanisms, fully kinetic particle-in-cell (PIC) simulations with the Aladyn code[29] in the 2D Cartesian geometry were carried out. The laser pulse was modeled by a Gaussian beam profile in the transverse coordinate with a FWHM spot size of 10 μm. The temporal profile on the focal plane was of the form $I(t) = I_0 \cos^4(\pi t/2\tau)$, where $2\tau = 70$ fs corresponding to a pulse duration of $\tau_{FWHM} = 25$ fs. The laser pulse entered into the computational (X, Y) box from the left edge, with an incidence angle of 30° with respect to the target normal. The dimensions of the numerical box were set to $L_X = 40$ μm and $L_Y = 50$ μm while the grid cell dimensions were set to dx = dy = 10 nm, thus allowing for reasonable space-time resolution. The initial density of Si^{4+} ions was set to $n_{Si} = 4 \times 3 \times 10^{22}$ cm^{-3}, corresponding to the plasma electron density $n_e = 100\, n_c = 1 \times 74 \times 10^{23}$ cm^{-3}. 256 (macro) electrons were used per cell in the PIC code. In modeling the laser-plasma interaction, field ionization using the Ammosov-Delone-Krainov (ADK) model was used. For the intensities considered here, the degree of ionization of Si ions increases from the initial Z = 4 to a final Z = (8–10).

In the case of plane silicon, p-polarization of the laser produces a mixing of a traveling wave structure (traveling parallel to the target surface) and a standing wave pattern along the x-direction.

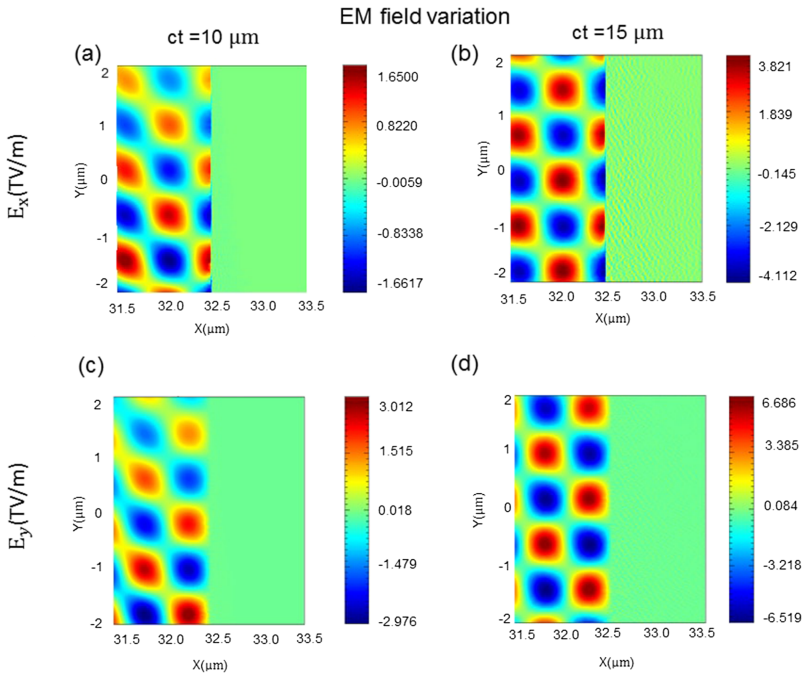

FIG. 3. Simulations for the EM field variations across the plane Si targets. The peak of the laser pulse impinges at t = 48 fs, corresponding to ct = 15 μm [(b) and (d)]. Therefore ct = 10 μm [(a) and (c)] corresponds to t = 30 fs.

This is well visible by observing the electromagnetic (EM) fields at two different times, corresponding to the leading part and peak of the pulse, showing that the horizontal nodes move in the y-direction while the vertical nodes are located at fixed distances from the target surface (Fig. 3); the electric field E_X (~3.4 TV/m at t = 48 fs) is maximum at the target surface and results in the extraction of electrons from the target. The larger electric field $2E_{0Y}$ (~6 TV/m), on the other hand, is localized far from the surface, at a distance $\approx\lambda_0 \cos(30^\circ)/4 \approx 175$ nm. This field is produced by the interference of the incident and the reflected laser and can accelerate the electrons to energies much higher than their mean oscillation energies in the laser electric field. Since the quiver amplitude of electrons $x_{quiver} \approx \frac{v_0\lambda_0}{4c} \sim 150$ nm, where $\frac{v_0}{c} = \sqrt{\frac{a_0^2}{a_0^2+1}}$, a few electrons are able to make it to the point of maximum E_Y, upon which they are accelerated at the maximum energy $E_{max} \approx (\sqrt{1+2a_0^2} - 1)m_ec^2 \approx 590$ keV. This model, similar to that introduced by May[30] and Kemp[31] for the interaction at normal incidence on a steep, overdense target, is in qualitative agreement with the maximum energy electrons obtained in the simulations and the experiment.

The nanowires were modeled by wires of size 20 nm separated by a gap of 40 nm. Unlike the real target, the nanowires in the model have a regular distribution on the surface. For a pulse with a normalized vector potential $a_0 = 1.4$, the PIC spectra for the front electrons exhibit a low flux of electrons with energy $E \leq 500$ keV and a high-energy tail with $E \geq 800$ keV in the normal direction (red curve, Fig. 4), features not observed in the experiment. Interestingly, the high energy tail strongly reduces on letting the 2D PIC simulations account for the formation of low density plasma in the channels prior to the arrival of the main pulse due to the temporal structure of the laser beam (blue curve, Fig. 4). This suggests that the high energy electrons are possibly generated by direct laser acceleration (DLA) into the channel gaps. This hypothesis is strengthened by performing 3D PIC simulations. In the 3D geometry, due to the low fill factor, the channels are no longer present and DLA becomes less efficient, resulting also in a reduction of high energy electrons (black curve, Fig. 4). Both the pre-plasma and 3D geometry, therefore, contribute to inhibit DLA acceleration, making the PIC spectra approach the experimental ones.

The observation of the spatial EM field distribution shows that, for negligible plasma formation prior to the main pulse, the laser initially penetrates the gap between the wires; owing to the formation of a strong spatial modulation resembling a fine tooth-comb at the target surface [Fig. 5(a)] there is an evident field enhancement resulting in large absorption of the laser energy. Due to the strong reduction of laser light reflection, there is no clear formation of a standing wave pattern and the EM field at the target front has the nature of a traveling wave along the incidence direction [Fig. 5(a)]. Similarly, due to the absence of the plasma between the channels, laser light travels between the wires, as visible in the figure. The situation is very different in the trailing part of the pulse, when the partial filling of the gaps by the plasma inhibits laser propagation into the target and

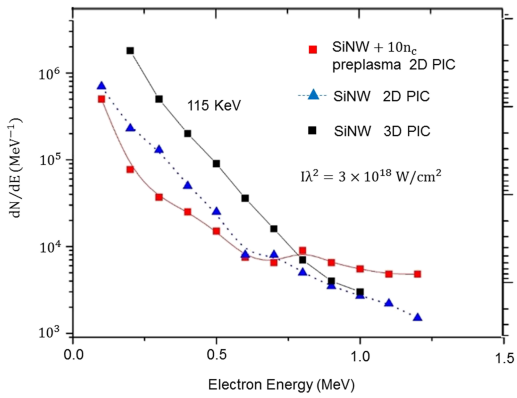

FIG. 4. 2D and 3D PIC electron energy spectra for the SiNW targets with no pre-plasma and in the presence of a pre-plasma of density 10 n_c.

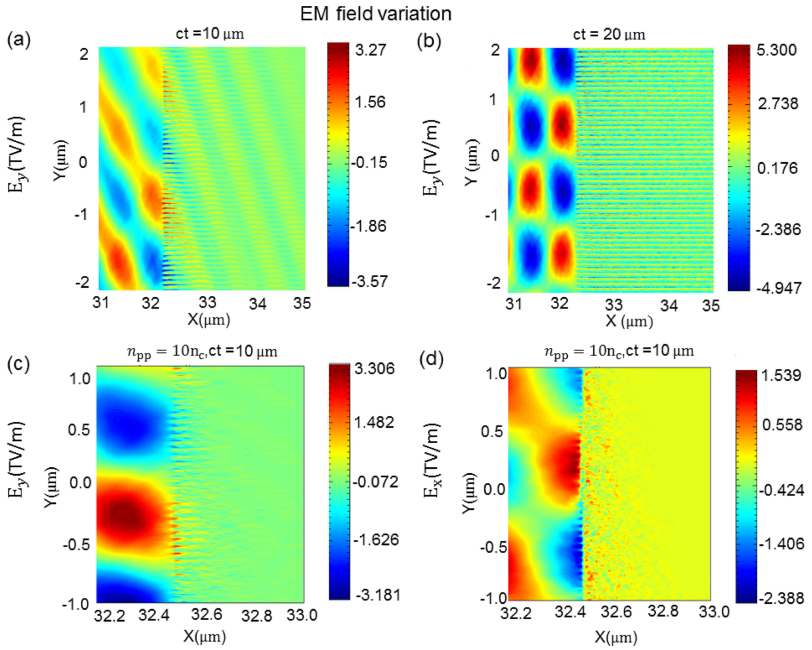

FIG. 5. Simulation figures of the EM field pattern in the nanowires in the absence [(a) and (b)] and presence [(c) and (d)] of the pre-plasma. Here ct = 10 and 20 μm correspond to t = 30 and 66 fs, respectively, and refer to early and late times of interaction.

the electrostatic fields between the wires are produced by charge separation [Fig. 5(b)]; owing to a large reflection at this time, a clear standing wave pattern is visible in front of the target along the x-direction [Fig. 5(b)].

In the real situation, a tenuous, low density plasma prior to the arrival of the main peak is already present between the wires due to the structure of the laser pulse. A strong spatial modulation and field enhancement, in the form of a fine-toothed comb [Fig. 5(c)], is however still present in a layer of approximately 100 nm leading to a more efficient laser absorption than in the case of the plane silicon target. The standing wave pattern at the target front gives rise to relativistic electrons with an energy distribution similar to that for plane silicon; however, the flux is higher in this case due to larger absorption. In this case, the EM field between the wires is prevailingly along the y direction [Fig. 5(c)], while the E_x component is inhibited by the pre-plasma [Fig. 5(d)]. This could result in the propagation of hot electrons primarily at larger angles, in agreement with the anisotropic distribution observed, even if an accurate investigation of the hot electron trajectory, accounting for magnetic fields, is required. The extent to which the electrons extracted from the wires can be accelerated by the laser field depends upon the closeness of the nanowires, as the oscillating phase is lost (upon reaching the neighboring wire) for separations less than the quiver amplitude. We therefore expect an optimization of the electron acceleration by tuning the gap between the nanowires.[32]

V. CONCLUSION

In summary, we show silicon nanowire arrays to be an extremely efficient absorber of laser energy and capable of generating relativistic electron pulses in the energy range of 0.2–0.8 MeV with a 30 times higher yield than that of the plane surface. Particle-in-cell (PIC) simulations of the interaction process reveal the role of the temporal structure of the laser pulse in the acceleration mechanism. It is seen that in the presence of an appreciable picosecond pedestal, the nanowire gaps are rapidly filled with the pre-plasma which hinders direct laser acceleration (DLA) of the electrons into the channels. Such relativistic electron beams show potential for applications in the study of ultrafast processes in biology, chemistry, and condensed matter physics.

ACKNOWLEDGMENTS

G.R.K. acknowledges support from the J. C. Bose Fellowship Grant (No. JCB-037/2010) from the Department of Science and Technology, Government of India. We also acknowledge the National Research Council of Italy for the support in the framework of the Short Term Mobility program 2014. This work was partially supported by the MIUR-PRIN 2012 (Contract No. PRIN2012AY5LEL) and by the INFN L3IA Project (No. CN5).

[1] L. Gremillet, F. Amiranoff, S. Baton, J.-C. Gauthier, M. Koenig, E. Martinolli, F. Pisani, G. Bonnaud, C. Lebourg, C. Rousseaux, C. Toupin, A. Antonicci, D. Batani, A. Bernardinello, T. Hall, D. Scott, P. Norreys, H. Bandulet, and H. Pépin, Phys. Rev. Lett. **83**, 5015(1999).
[2] G. Chatterjee, P. K. Singh, S. Ahmed, A. P. L. Robinson, A. D. Lad, S. Mondal, V. Narayanan, I. Srivastava, N. Koratkar, J. Pasley, A. K. Sood, and G. R. Kumar, Phys. Rev. Lett. **108**, 235005 (2012).
[3] P. K. Singh, G. Chatterjee, A. D. Lad, A. Adak, S. Ahmed, M. Khorasaninejad, M. M. Adachi, K. S. Karim, S. S. Saini, A. K. Sood, and G. Ravindra Kumar, Appl. Phys. Lett. **100**, 244104 (2012).
[4] I. Dey, A. Adak, M. Shaikh, G. Chatterjee, D. Sarkar, A. D. Lad, and G. Ravindra Kumar, Opt. Express **24**, 28419 (2016).
[5] A. Adak, P. K. Singh, A. D. Lad, G. Chatterjee, M. Dalui, P. Brijesh, A. P. L. Robinson, J. Pasley, and G. Ravindra Kumar, Appl. Phys. Lett. **109**, 174101 (2016).
[6] Y. Zhang, N. K. Grady, C. Ayala-Orozco, and N. J. Halas, Nano Lett. **11**, 5519 (2011).
[7] C. E. Talley, J. B. Jackson, C. Oubre, N. K. Grady, C. W. Hollars, S. M. Lane, T. R. Huser, P. Nordlander, and N. J. Halas, Nano Lett. **5**, 1569 (2005).
[8] K. Kneipp, Y. Wang, H. Kneipp, L. T. Perelman, I. Itzkan, R. R. Dasari, and M. S. Feld, Phys. Rev. Lett. **78**, 1667 (1997).
[9] G. Ispasoiu, L. Balogh, O. P. Varnavski, D. A. Tomalia, and T. Goodson III, J. Am. Chem. Soc. **122**, 11005 (2000).
[10] M. A Purvis, V. N. Shlyaptsev, R. Hollinger, C. Bargsten, A. Pukhov, A. Prieto, Y. Wang, B. M. Luther, L. Yin, S. Wang, and J. J. Rocca, Nat. Photonics **7**, 796 (2013).
[11] S. Mondal, I. Chakraborty, S. Ahmad, D. Carvalho, P. K. Singh, A. D. Lad, V. Narayanan, P. Ayyub, G. R. Kumar, J. Zheng, and Z. M. Sheng, Phys. Rev. B **83**, 035408 (2011).
[12] D. K. Polyushkin, E. Hendry, E. K. Stone, and W. L. Barnes, Nano Lett. **11**, 4718 (2011).
[13] D. Margarone, O. Klimo, I. J. Kim, J. Prokůpek, J. Limpouch, T. M. Jeong, T. Mocek, J. Pšikal, H. T. Kim, J. Proška, K. H. Nam, L. Štolcová, I. W. Choi, S. K. Lee, J. H. Sung, T. J. Yu, and G. Korn, Phys. Rev. Lett. **109**, 234801 (2012).
[14] S. Bagchi, P. Prem Kiran, M. K. Bhuyan, S. Bose, P. Ayyub, M. Krishnamurthy, and G. Ravindra Kumar, Appl. Phys. Lett. **90**, 141502 (2007).
[15] F. Légaré, K. F. Lee, A. D. Bandrauk, D. M. Villeneuve, and P. B. Corkum, J. Phys. B: At., Mol. Opt. Phys. **39**, S503 (2006).
[16] E. R. Keim, M. L. Polak, J. C. Owrutsky, J. V. Coe, and R. J. Saykally, J. Chem. Phys. **93**, 3111 (1990).
[17] S. V. Bulanov and V. S. Khoroshkov, Plasma Phys. Rep. **28**, 453 (2001).
[18] V. Malka, J. Faure, Y. A. Gauduel, E. Lefebvre, A. Rousse, and K. T. Phuoc, Nat. Phys. **4**, 447 (2008).
[19] S. Cabrini, A. Carpentiero, R. Kumar, L. Businaro, P. Candeloro, M. Prasciolu, A. Gosparini, C. Andreani, M. De Vittorio, T. Stomeo, and E. Di Fabrizio, Microelectron. Eng. **78–79**, 11 (2005).
[20] P. P. Rajeev, P. Taneja, P. Ayyub, A. S. Sandhu, and G. R. Kumar, Phys. Rev. Lett. **90**, 115002 (2003).
[21] S. Jiang, A. G. Krygier, D. W. Schumacher, K. U. Akli, and R. R. Freeman, Eur. Phys. J. D **68**, 283 (2014).
[22] G. Cristoforetti, A. Anzalone, F. Baffigi, G. Bussolino, G. D'Arrigo, L. Fulgentini, A. Giulietti, P. Koester, L. Labate, S. Tudisco, and L. A. Gizzi, Plasma Phys. Controlled Fusion **56**, 95001 (2014).
[23] L. Hu and G. Chen, Nano Lett. **7**, 3249 (2007).
[24] P. P. Rajeev, P. Ayyub, S. Bagchi, and G. R. Kumar, Opt. Lett. **29**, 2662 (2004).
[25] D. Strickland and G. Mourou, Opt. Commun. **55**, 447 (1985).
[26] A. Tarasevitch, C. Dietrich, C. Blome, K. Sokolowski-Tinten, and D. von der Linde, Phys. Rev. E **68**, 26410 (2003).
[27] L. Veisz, W. Theobald, T. Feurer, H. Schillinger, P. Gibbon, and P. Sauerbrey, Phys. Plasmas **9**, 3197 (2002).
[28] K. A. Tanaka, T. Yabuuchi, T. Sato, R. Kodama, Y. Kitagawa, T. Takahashi, Y. Honda, and S. Okuda, Rev. Sci. Instrum. **76**, 13507 (2004).
[29] C. Benedetti, A. Sgattoni, G. Turchetti, and P. Londrillo, IEEE Trans. Plasma Sci. **36**, 1790 (2008).
[30] J. May, J. Tonge, F. Fiuza, R. A. Fonseca, L. O. Silva, C. Ren, and W. B. Mori, Phys. Rev. E **84**, 25401 (2011).
[31] G. E. Kemp, A. Link, Y. Ping, D. W. Schumacher, R. R. Freeman, and P. K. Patel, Phys. Plasmas **20**, 33104 (2013).
[32] G. Cristoforetti, P. Londrillo, P. K. Singh, F. Baffigi, G. D'Arrigo, A. D. Lad, R. G. Milazzo, A. Adak, M. Shaikh, D. Sarkar, G. Chatterjee, J. Jha, M. Krishnamurthy, G. R. Kumar, and L. A. Gizzi, Sci. Rep. **7**, 1479 (2017).